Reversible metallisation of soft UV patterned substrates

Panida Prompinit,[†] Ammathnadu S. Achalkumar,[‡] Mark C. Robbins,[§] Alexander S. Walton,[≠]

Richard J. Bushby,[‡] Christoph Wälti,[§] and Stephen D. Evans[*,†]

[≠†] Molecular and Nanoscale Physics, School of Physics and Astronomy, University of Leeds,

Leeds, LS2 9JT, UK

[≠‡] School of Chemistry, University of Leeds, Leeds, LS2 9JT, UK

[§§] Institute of Microwaves and Photonics, School of Electronic and Electrical Engineering,

University of Leeds, Leeds LS2 9JT, UK

ABSTRACT:

Soft UV (365 nm) patterning of *ortho*-nitrobenzyl functionalized thiol-on-gold self-assembled monolayers (SAMs) using acid catalysis, produces surfaces which can be used for the selective electro-deposition of copper. Exploiting the difference in the reduction peak potential between the photolyzed and the masked regions of the SAM allows copper to be deposited selectively on those areas that have been exposed to the light. The copper can be removed by raising the electrode potential. The process is fully reversible so that depositing a pattern of copper and removing it again is something that can be repeated many times. The copper deposited on the photolyzed regions, like copper deposited on bare gold, forms a film of copper oxide, and so it is presumably formed on top of the SAM. Preliminary results for two-photon photocleavage suggest that it is also possible to implement patterning with sub-wavelength features.

1. INTRODUCTION

The use of self-assembled monolayers (SAMs) to direct metal deposition has received significant attention in recent years.[1] Potential applications include the fabrication of metal-SAM-metal junctions[2-4] and the formation of metallic clusters both for localization of plasmonic effects[5] and for surface-enhanced spectroscopies.[6,7] Patterned SAMs can also be used for the selective growth of metal nanostructures,[8] thin free-standing metal /magnetic films,[9] and for mold and replica fabrication.[10,11] Electrochemical deposition (ECD) is the simplest technique for depositing the metal being low-cost and compatible with complex patterning and manufacturing procedures.[8,12] To date a variety of SAM modified electrodes has been used including *n*-alkanethiol and ω-functionalised alkanethiol SAMs[13-19] as well as SAMs made using phenyl, biphenyl and heterocyclic thiols.[19-26] In order to direct metal deposition, SAMs have been patterned by micro-contact printing,[27-29] deep UV photolithography[8,12,20,24,30] or E-beam lithography.[31] The use of soft UV (365 nm) photolithography of *ortho*-nitrobenzyl protected SAMs provides a potentially attractive alternative since this offers much greater control over the chemical functionality of the surface.[32-34] Recently, we have shown that it is possible to obtain photolysis yields of ~ 95% for the soft UV deprotection of *ortho*-nitrobenzyl-based SAMs, provided acid catalysis is employed.[35,36] Compared to deep UV photolithography, soft UV lithography also has the advantage that it can be used for patterning that overcomes the diffraction limit by exploiting two-photon photochemistry.[37-43] In this paper we use thiol-on-gold SAMs, acid-catalyzed soft UV photolithography and also two-photon soft UV lithography to create patterned SAMs coupled with ECD to deposit copper on the photo-deprotected regions of the surface in a reversible, repeatable manner

2. EXPERIMENTAL SECTION

2.1. Synthesis of ester 1. 4,4′-Dithiodibutyric[4-(1H,1H,2H,2H-perfluorooctyloxy)-5-methoxy-2-nitrobenzyl] ester **1** (Figure 1a) was synthesized as previously described and had physical and spectroscopic properties in accordance with those previously reported.[34,35]

2.2. SAM formation. Ester **1** and 4,4′-dithiodibutyric acid (DTBA) **2**, SAMs were formed by immersing the gold-coated slides in 0.5 mM solutions of the corresponding compound, in

dichloromethane (DCM), for 16 h, at 23 °C. The samples were then removed, rinsed with DCM, dried with a stream of nitrogen, rinsed with Milli-Q water, and again dried.

2.3. UV irradiation/single-photon photopatterning. For the single-photon patterning process, filtered soft-UV (365 nm) light was obtained from the fluorescence microscope (Nikon) with a power (at the sample) of 40 mW·cm^{-2}. Patterning of the SAM was done by irradiating samples for 5 min (12 J·cm^{-2}) under 0.1 M HCl/isopropanol through a photomask. After UV irradiation, samples were rinsed with DCM, followed by Milli-Q water and finally they were dried using a stream of nitrogen.

2.4. Electrochemical deposition (ECD). The electrochemical deposition was performed using the SAM modified gold electrode as the working electrode, a coil of platinum wire as the counter electrode with a Ag/AgCl reference electrode. The electrolyte solution was 10 mM aqueous $CuSO_4$ in 10 mM H_2SO_4. The ECD was performed using an Autolab PG30 potentiostat. The cyclic voltammograms (CVs) were recorded in the range between -0.30 V and +0.40 V at a scan rate of 10 mV·s^{-1}. The appropriate deposition potential for the copper was determined from the CV.

2.5. High resolution two-photon patterning. Two photon patterning was achieved using a confocal laser scanning microscope (Olympus Fluoview FV-1000, Japan) coupled to a Ti-sapphire laser (Mai Tai, Spectra Physics, Inc., USA). The Mai Tai laser is tunable in the range of 780-920 nm and provides ~80 fs pulses at a repetition rate of 80 MHz. The maximum time-averaged laser power in the object plane at 780 nm wavelength was about 0.12 W, corresponding to a pulse energy of roughly 1.5 nJ. These photolyses were carried out directly in the air without using acid catalysis.

2.6. Atomic Force Microscopy (AFM). The AFM images of copper deposited on SAMs were acquired at ambient conditions by using a Nanoscope IIIa MultiMode AFM (Veeco Instruments, Santa Barbara, CA). Samples were scanned to provide topographic information with AFM contact mode tips (Si_3N_4) attached to a cantilever with a nominal spring constant of 0.06 N/m.

2.7. Scanning Electron Microscopy (SEM). SEM measurements were taken using a Zeiss Gemini 1500 UHV FEGSEM attached to an Omicron Nanoprobe system. The micrographs were taken at an accelerating voltage of 8 kV and a probe current of 100 pA.

3. RESULTS AND DISCUSSION

3.1. SAM formation and photoylsis. The disulphide **1** (Figure 1a) was used to create **SAM1** which has a terminal perfluorocarbon chain. On exposure to soft UV light (365 nm) the O/C (ester oxygen/benzylic carbon) bond is cleaved giving **SAM2** which is terminated with a COOH group (Figure 1b).[34,35] Although photo-deprotection of *ortho*-nitrobenzyl esters in dilute solution is typically a high-yielding reaction (98-99%), the yield from direct photolysis of *ortho*-nitrobenzyl functionalized SAMs is known to be poor (~50%).[32,34,36] Much better yields (~95%) are obtained when they are photolyzed through a layer of 0.1M HCl in IPA.[36] Although **SAM2** made by 0.1M HCl in IPA catalyzed photolysis of **SAM1** is structurally similar to that produced when 4,4′-dithiodibutyric acid (**2**, DTBA) is reacted with the gold there are some differences that may be significant so far as metal deposition is concerned.[32,36] Firstly, because of the steric bulk of the *ortho*-nitrobenzyl protecting group, the SAM formed photochemically will be less densely packed. The SAM produced from the disulphide **1** is typically 14.3 ± 0.4 Å thick. Using a molecular volume of 451 $Å^3$ for $C_{20}H_{17}F_{13}NO_6S$ gives an estimated area per thiolate of 31-32 $Å^2$ for **SAM1** and hence for **SAM2** produced by photolysis of **SAM1**. On the other hand **SAM2** produced from the disulphide **2** has an estimated thickness of ~5.6 Å and using a molecular volume of 108 $Å^3$ for $C_4H_7O_2S$ then gives an estimated area per thiolate of 19 $Å^2$.[32] Although these are quite rough estimates it is clear that **SAM2** produced by photolysis of **SAM1** is substantially less densely packed than that made from DTBA. Secondly, although the chemical yield for the acid catalyzed photolysis reaction is ~95% it is not 100%. As a result, at the end of the photolysis, there will be ~5% by-product bound to the surface. This by-product is probably mostly material in which the *ortho*-NO_2 group has been reduced to an *ortho*-NH_2 or *ortho*-NO group.[32] The fact that the **SAM2** is less densely packed when it is produced by photolysis of **SAM1** will aid selective ECD whereas the presence of bound by-products will hinder the process.
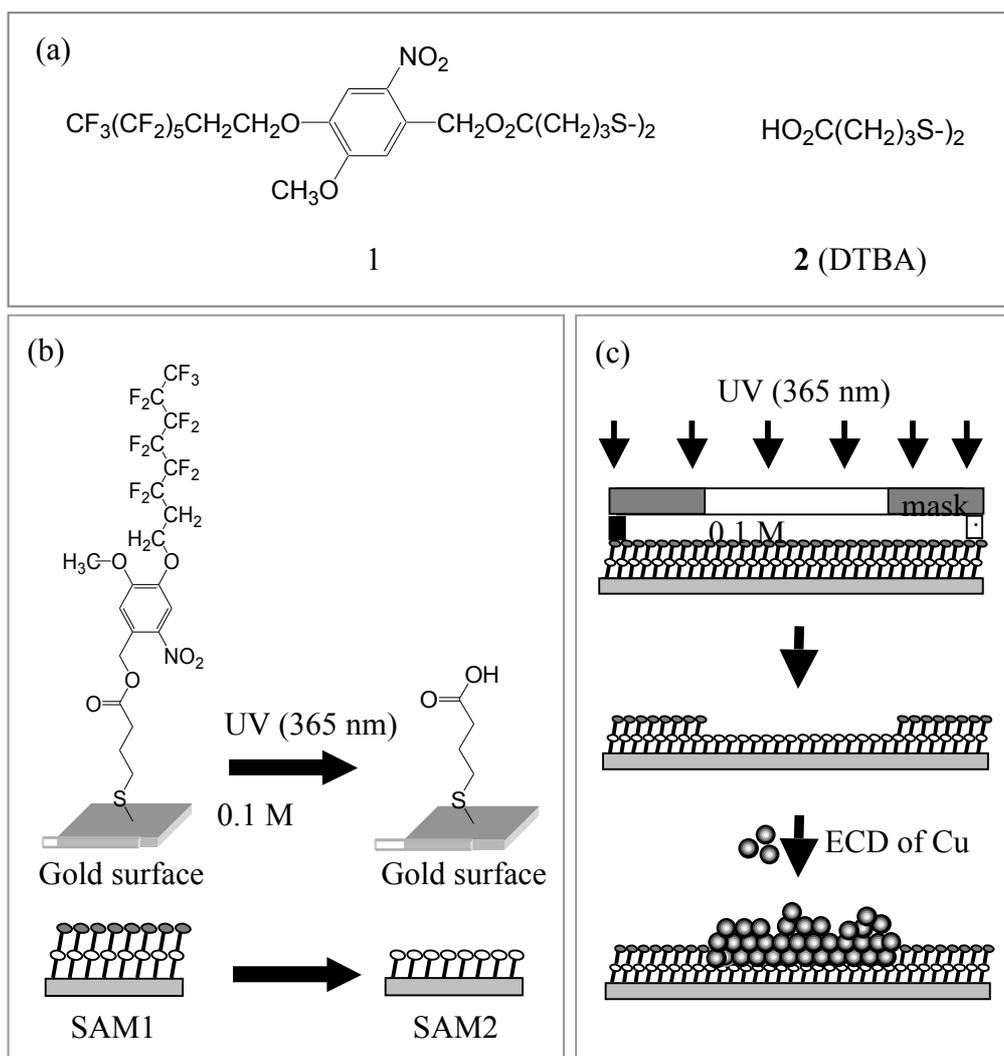
Figure 1. (a) Molecular formulae of the SAM-forming disulphides used in this study. (b) Schematic of the photo-deprotection **SAM1** under soft UV (365 nm) irradiation in 0.1 M HCl isopropanol. (b) Schematic of the photo-patterning of **SAM1** through a mask followed by electrochemical deposition (ECD) of copper.
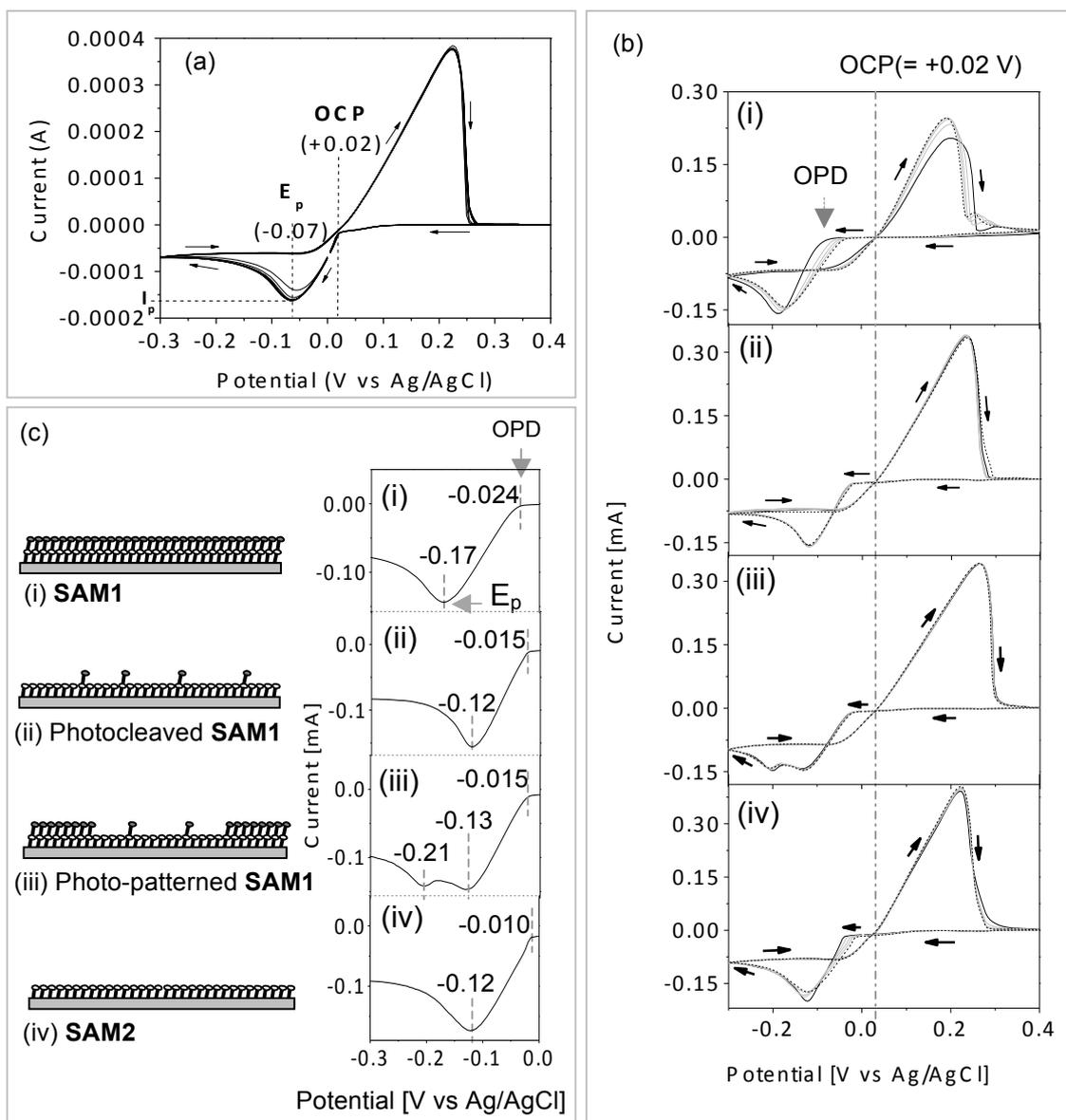
Figure 2. (a) Plot of ten cycles of the cyclic voltammogram (CV) relative to a Ag/AgCl reference electrode for 10 mM CuSO$_4$ in 10 mM H$_2$SO$_4$ above a clean gold surface (scan rate: 10 mV·s^{-1}). (b) Equivalent voltammograms for 10 mM CuSO$_4$ in 10 mM H$_2$SO$_4$ above (i) fresh **SAM1**, (ii) **SAM2** formed by photolysis of **SAM1**, (iii) photo-patterned **SAM1** (200 μm × 150 μm stripes), and (iv) **SAM2** formed directly from DTBA **2**. Ten CV cycles were taken for each sample (scan rate =10 mV·s^{-1}). The black line represents cycle 2, grey lines represent cycles 4, 6 and 8, and dashed line represents cycle 10. (c) Detail of the copper deposition region for each of the SAM functionalized surfaces. The 10th cycle is shown.

3.2. Reversible Copper Deposition and Stripping. A typical cyclic voltammogram for a bare gold electrode in aqueous 10 mM $CuSO_4$ in 10 mM H_2SO_4 is shown in Figure 2(a). The electrode potential was cycled between +0.40 V and -0.30 V at 10 mV·s^{-1}. This voltammogram did not show any significant changes after 10 voltammetric cycles. The open cell potential (OCP), the potential corresponding to the equilibrium between Cu^{2+} and Cu^0, was found to be 0.02 V. Cu^{2+} is reduced at potentials more negative than this to form Cu^0 and the copper film dissolves back into solution at potentials more positive than +0.2V. The maximum (negative) current in the reduction cycle (I_p) corresponds to a peak potential (E_p) of -0.07 V. Complete removal of the copper layer from the gold electrode was achieved at +0.40 V. Equivalent voltammograms for gold electrodes functionalized with four different SAMs are shown in Figure 2b. In each case, the overall form of the trace is very similar to that for bare gold but, relative to bare gold, the reduction of copper is shifted to a more negative potential. On **SAM1** deposition begins at -0.024 V (Figure 2c (i)) on **SAM2** obtained by photolysis of **SAM1** at -0.015 V (Figure 2c (ii)) on photo-patterned **SAM1** at -0.015 V (Figure 2c (iii)) and on **SAM2** obtained directly using DTBA at -0.010 V (Figure 2c (iv)). This is more-or-less the order expected for a penetration/ thickness-limited electron transfer process. The fact that the over-potential for the photo-patterned and photo-cleaved samples was about the same implies that, for the photo-patterned surface, the photo-cleaved regions dominate the process. The peak potentials, E_p, also decreased with decreasing SAM thickness as follows:- **SAM1** (-0.17 V) (Figure 2c (i)) > photocleaved **SAM1** (-0.12) (Figure 2c (ii)) = DTBA **SAM2** (-0.12 V) (Figure 2c (iv)). In the case of photo-patterned **SAM1** (Figure 2c (iii)), two separated peak potentials were observed at -0.13 V and -0.21 V corresponding, respectively, to the photoreacted and non-photoreacted regions of the surface. As a result, selective electro-deposition of copper can be directed to occur on the photocleaved regions by applying a constant negative potential of less than E_p (less than -0.21 V). For the data shown in Figure 3a (*left*) the potential for a patterned SAM was set at a constant value -0.10 V and the current and the mass of deposited copper were monitored as a function of time; the mass of deposited copper being calculated from the integrated area under the current-time curve. After the initial reaction period of ~ 20s, a constant deposition rate of ~2.59 × 10^{-8} g·s^{-1} was observed. As for the case of a bare gold electrode, the deposition behavior was found to follow the Cottrel equation, where the change of current is dependent on the square root of the diffusion coefficient of Cu^{2+} in the electrolyte.[44,45] This means that the reduction process is dominated by the diffusion rate of Cu^{2+} from the electrolyte to the electrode surface, rather than by the SAM. After deposition, gray scale plot profiles, which relate to the brightness of

copper deposited on surface, generated from optical microscopy images, showed high contrast on the patterned surface between photocleaved and non-reacted **SAM1** regions (Figure 3c). Following the deposition of copper on the photo-patterned SAM, the copper was subsequently removed from the surface by raising the potential to +0.40 V. Figure 3a (*right*) once again shows the decrease in current and mass of stripped copper as a function of oxidation time. There are two distinct regions for the oxidation reaction. Firstly, the region between 0 s and 7 s corresponds to almost constant current caused by the oxidation of copper, from the copper layer which was deposited on the SAM modified gold electrode surface. The stripping rate during this period was ~3.26×10^{-7} g·s^{-1}. Secondly, after 7 s, a sharp decrease in current occurred due to the depletion of the copper metal layer from the surface. The copper was completely removed from the sample after 20 s. The mass of both deposited and stripped copper were essentially the same ~ $(3.80 \pm 0.4) \times 10^{-6}$ g.

Perhaps the most interesting observation, for these SAM-coated electrodes, is that the deposition and stripping of the copper are reversible over many cycles. A movie showing the reversibility of the deposition and stripping of the copper over the first two cycles is included in the supplementary information. Figure 3d shows microscope images of an area of a patterned surface after 2 and after 37 CV cycles in which there was complete copper removal after each deposition step. Both the CV data (Figure 2b(iii)) and the visual evidence (Figure 3d and the movie) show that the nature and patterning of the SAM are essentially unaffected by copper deposition and copper removal. In an attempt to obtain a better understanding of this process, the nature of the deposited copper was further investigated by optical microscopy and also by AFM and by XPS and Auger spectroscopy. The latter suggest that the copper is deposited on top of the photolyzed SAM.

(a)

(b) Deposition at t = 0 s

Deposition at t = 140 s and stripping at t = 0 s

Stripping at t = 30 s

700 µm

(c)

Unreacted **SAM1**   Photocleaved **SAM1**

After deposition at -0.10 V for 140 s

Deposition at t = 0 s and stripping at t = 30 s

(d) 2nd cycle

37th cycle

(i)

(ii)

10
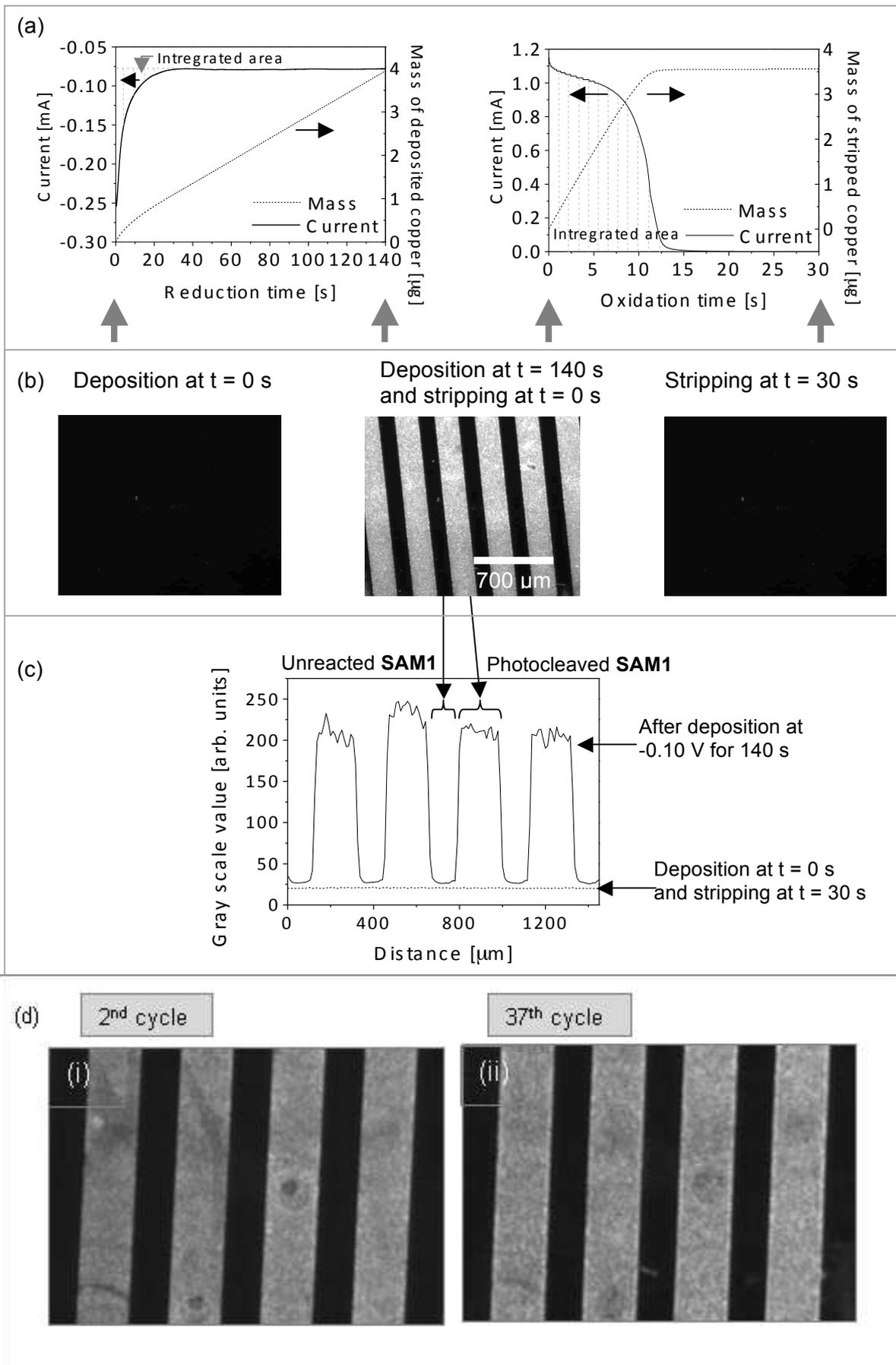
Figure 3. (a) Plots for the variation of the current and the mass of deposited/stripped copper on the photo-patterned **SAM1** as a function of reduction/oxidation time at -0.1V and +0.4V in 10 mM $CuSO_4$, 10 mM H_2SO_4. (b) Optical microscope images showing the metallisation. The images were taken at before (t = 0 s) and after deposition at -0.10 V for 140 s. The copper metal selectively grew on the photocleaved **SAM1** areas (bright regions, 200 μm stripes) whereas no or very little copper was observed on the unreacted **SAM1** (dark regions, 150 μm stripes). The deposited copper was removed at +0.40 V for 30 s. (c) The grey-scale plot profiles showing the deposited copper on patterned **SAM1** formed at -0.10 V for 140 s. (d) Microscope images of the copper deposited on a photo-patterned SAM (200 μm wide stripes) after (i) the 2nd cycle and (ii) the 37th cycle
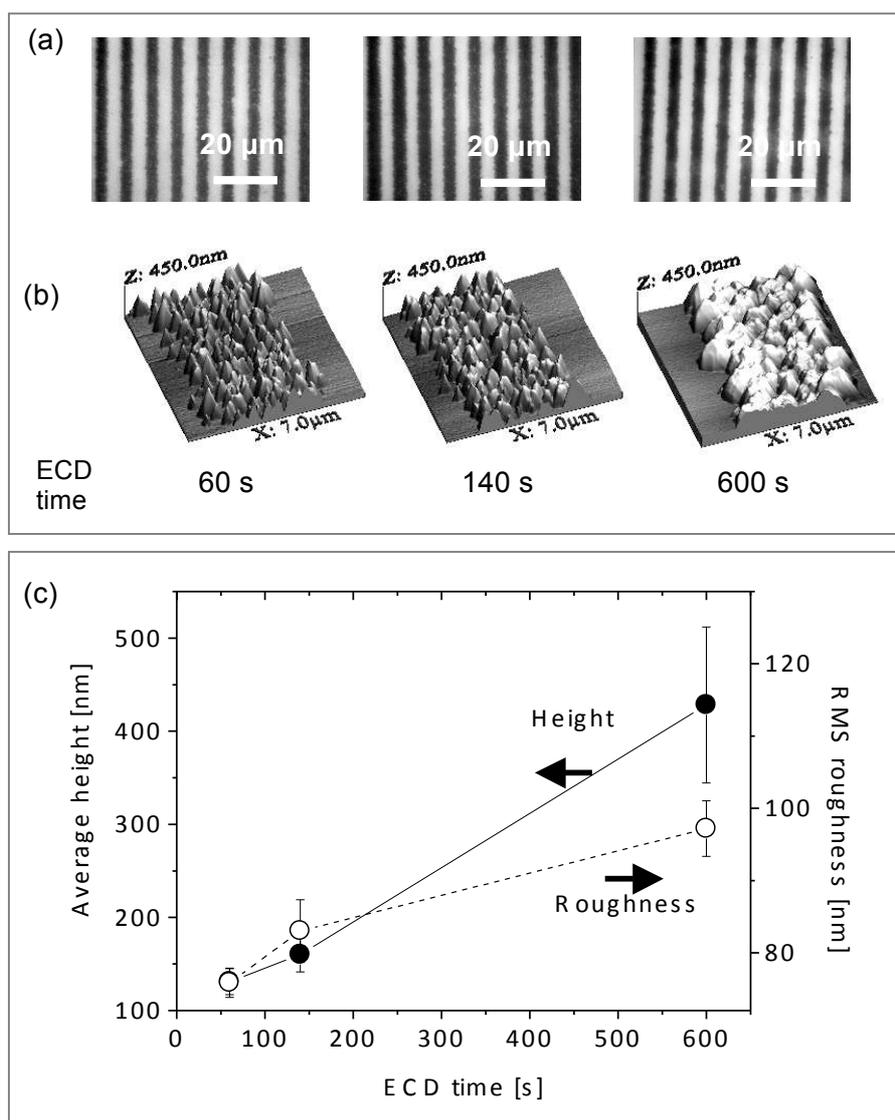
**Figure 4.** (a) Optical images and (b) contact mode AFM (height) images of the copper grown at -0.08 V for 60s, 140s, and 600s, on photocleaved regions of photopatterned **SAM1** with 5 μm wide stripes. (c) Average height over a 7 × 7 μm^2 area (left scale, solid line) and RMS roughness measured over a 2.5 × 2.5 μm^2 area (right scale, dashed line: guide to the eye) at the centre of copper at these times.

The growth of the copper layer during the deposition process was investigated by optical microscopy and typical images are shown in Figure 4a. AFM images of the copper layer after growth for 60, 140 and 600 s are shown in Figure 4b. In the early stages of the deposition (after reduction for 60 s or for 140 s) there was no apparent difference in the density of copper particles as a function of time implying that the nucleation did not change. At longer ECD times (e.g. reduction for 600 s), the copper particles began to merge. It was always found that the copper particles along the edge of striped pattern were larger than those in the centre of the stripe. This is probably caused by the difference in diffusion fields. At the centre of the stripe, copper deposition is limited by linear diffusion of Cu^{2+} from the bulk solution immediately above the electrode but at the edge there is an additional radial contribution to the diffusion field from the regions above the unphotolyzed stripe. After an initial period of rapid growth the height of the deposited copper increases in a roughly linear manner (see Figure 4c). As shown, the RMS roughness also increases with time.
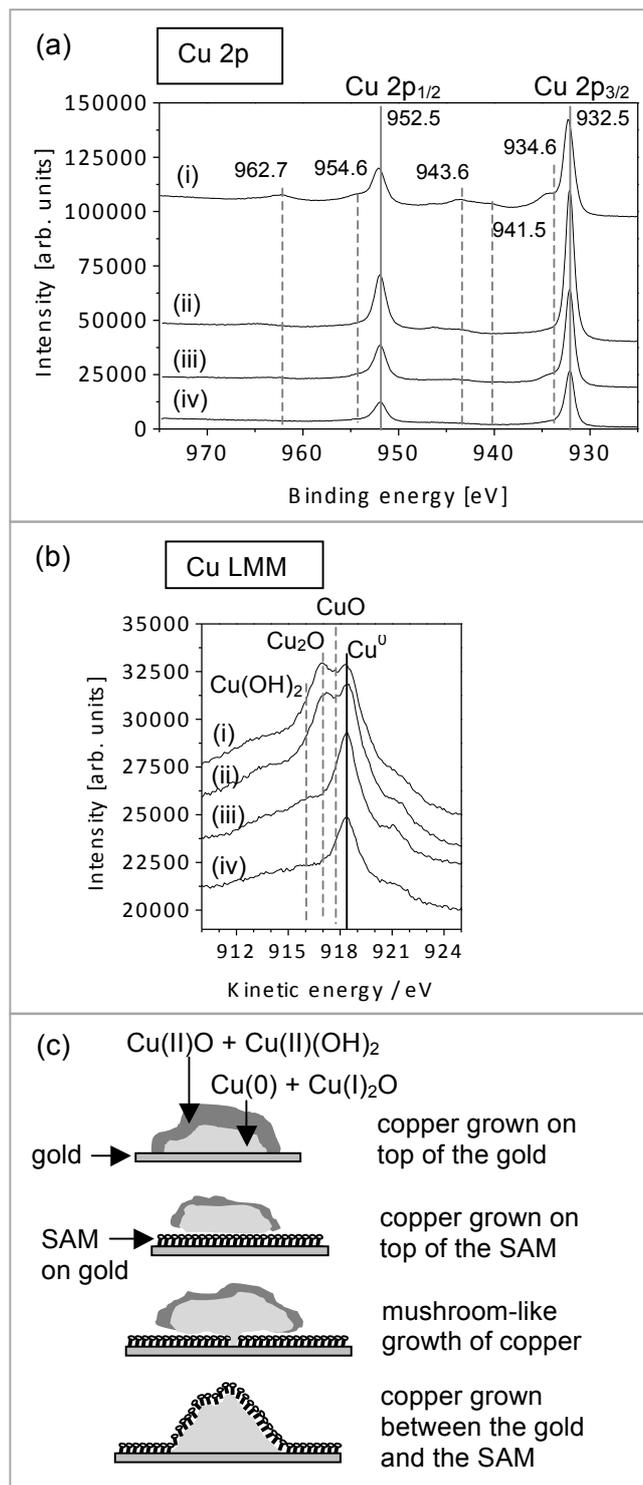
Figure 5. (a) Cu 2p XPS spectra of copper deposited on different substrates (i) bare gold surface; (ii) photocleaved **SAM1**; (iii) DTBA SAM; and (iv) **SAM1**. The solid line represents the position expected for Cu^0 and Cu^{1+} species. The dash line represents the position for Cu^{2+} species. (b) Cu LMM Auger spectra of copper deposited on these surfaces. (c) Schematic of possible modes of copper deposition on bare gold and SAM modified gold surfaces (see text).

XPS and Auger spectroscopy were used to investigate the copper deposited on **SAM1**, on **SAM2** formed by direct reaction of the gold with DTBA **2**, on **SAM2** produced by photolysis of **SAM1**, and also copper deposited on a 'bare' gold electrode. In the first two cases, the cases involving densely packed SAMs, there was little evidence for atmospheric oxidation of the copper layer but in the second two cases, and particularly in the case of 'bare' gold, oxidation clearly occurred.

In these samples, the XPS spectra for the Cu 2p region (Figure 5a) show two main peaks at 932.5 eV and 952.5 eV corresponding to Cu $2p_{3/2}$ and Cu $2p_{1/2}$, respectively, and these could correspond to either metallic copper[49-53] or Cu^{1+}.[49-55] These oxidation states are difficult to distinguish by XPS.[56] However, the shake-up peaks in the range of 938.0 – 945.0 eV for Cu $2p_{3/2}$ and at 962.7 eV for Cu $2p_{1/2}$, are characteristic of Cu^{2+}. These are observed for the copper deposited on the bare gold surface[49,54,57] and they are weakly present for the copper deposited on photocleaved **SAM1** (Figure 5a(i) and 5a(ii)). However, they are absent for the copper deposited on **SAM2** made from DTBA and for copper deposited on **SAM1** (Figure 5a(iii) and 5a(iv)). The broad peak at 934.6 eV, which is identified as $Cu(OH)_2$,[49,50,52,54,55] was observed in the case of the copper deposited on bare gold and, more weakly, in the case of **SAM2** made from DTBA (Figure 5a(i) and 5a(iii)). Overall the Cu 2p region suggests that the main oxidation state of the copper deposited on all surfaces could be either Cu^0 (metallic copper) or Cu^{1+} (Cu_2O). Cu^{2+} (CuO and $Cu(OH)_2$) was certainly present for the copper deposited on bare gold and in small amounts for the copper deposited on photocleaved **SAM1**. There also appear to be small amounts of $Cu(OH)_2$ in the copper deposited on **SAM2** made from DTBA.

In the Cu LMM Auger spectral regions (Figure 5b), the four main peaks observed for copper deposited on the bare gold surface, at 916.0 eV, 917.0 eV, 917.7 eV and 918.2 eV correspond to $Cu(OH)_2$, Cu_2O, CuO, and Cu metal, respectively.[50,52,54,55] The oxidation state of the copper deposited on **SAM1** and on **SAM2** produced from DTBA was Cu^0 (Figure 5b(iii) and 5b(iv)). Clear evidence is seen for Cu^0, Cu^{1+} (Cu_2O) and Cu^{2+} (CuO and $Cu(OH)_2$)) for the copper deposited on bare gold and for the copper deposited on **SAM2** formed by photolysis of **SAM1** (Figure 5b(i) and 5b(ii)). The broad peak at ~916.0 eV for the copper deposited on **SAM2** formed from DTBA confirms the presence of small amounts of $Cu(OH)_2$. Overall these results confirm those obtained by XPS but perhaps give a clearer indication for oxidation of the copper deposited on the photolyzed SAM.

In the deposition process, electron transfer can occur through defect sites, or directly across the SAM, leading to a metallic copper layer on top of the SAM.[18] Alternatively, if the Cu^{2+}

penetrates through the defect sites to the surface of the gold, the copper can grow from the surface leading to nanometer-sized columns and subsequently 'mushroom-shaped' growths.[11,31,46] In both cases the copper surface is exposed to air and it is expected that this will lead to the formation of a thin film of copper oxide. A third possibility is that the growth proceeds through penetration of Cu^{2+} through the defects leading to a copper layer between the gold and the thiol.[14,20] In this case the copper is covered by the thiol SAM and oxide formation should be reduced. These various possibilities are illustrated schematically in Figure 5c.

The absence of oxidation, for the densely packed SAMs (**SAM1** and **SAM2** formed from DTBA), suggest that the copper is protected from the air and that it is deposited between the thiol and the gold.[47,48] However, when **SAM2** is formed by photolysis of **SAM1** it is less densely packed and also it probably contains more defect sites. In this case the deposited copper is similar to that deposited on bare gold. In addition to the presence of metallic copper (Cu^0) both Cu(I) and Cu(II) oxide states (CuO, Cu_2O, $Cu(OH)_2$) are seen suggesting that the Cu is deposited above the SAM.

Unfortunately it is not possible to confirm this hypothesis by using the S 2p peak for sulfur bound to copper because this is very close to that for gold-bound sulfur[49,50,58]

3.3. Two photon patterning of the surface. The 'soft UV' method for creating patterned SAMs can be used to generate patterned surface with a resolution better than the wavelength of the light if two-photon photolysis is employed. Álvarez *et al* have recently demonstrated a two photon (λ = 780 nm) cleavage of *ortho*-nitrobenzyl units in silane-on-quartz SAMs [42,43] and so it should be possible to achieve two-photon photocleavage of the *ortho*-nitrobenzyl moieties in these thiol-on-gold SAMs. Photolyses were carried out directly (without an HCl/IPA catalytic layer). Two photon patterning of **SAM1** was achieved using a confocal laser scanning microscope coupled to a Ti-sapphire laser that provided ~80 fs pulses at a repetition rate of 80 MHz. A spiral (tornado) pattern was written on the surface which was subsequently decorated with copper using ECD. Typical results are shown in Figure 6. To ensure that the photolysis is the result of specific photo-patterning, rather than non-specific photo-oblation of the SAM layer, the experiment was repeated with **SAM2** made from DTBA. In this case a copper layer was observed covering the whole surface: no pattern of deposited copper was observed. Hence, the patterned surface obtained by photolysis of **SAM1** followed

by copper deposition shows that we are aceiving a two-photon process leading to specific photochemistry.

Figure 7 shows SEM images for copper deposited on a two-photon patterned **SAM1**, which was fabricated using different laser powers and irradiation times. Using a scan rate of 10 μs/pixel a low laser power (62.2 mW) and a short irradiation time (180 s) a structure with a low density of isolated long grain copper particles was observed on 700-800 nm wide stripes (Figure 7a). Increasing the laser power to 80.8 mW but with the same irradiation time, the density of the copper particles increased as did the stripe width (Figure 7b) and in the centre of the stripes merging of the copper particles was observed. Using a longer irradiation time at a lower laser power (62.2 mW) resulted in a high density of small copper particles (Figure 7c), perhaps suggesting a higher density of photocleaved molecules. At higher laser power (80.8 mW) and longer irradiation time (315 s), the whole patterned surface was covered by a continuous film of copper (Figure 7d). In these experiments we have only achieved a resolution of ~ 1μm but they establish the principle that two-photon lithography can be used for these SAMs and other workers have shown that two-photon lithography is capable of writing features which are < 0.1μm.[59] The combination of laser power and irradiation appear to be sensitive parameters for tuning particle/film growth.
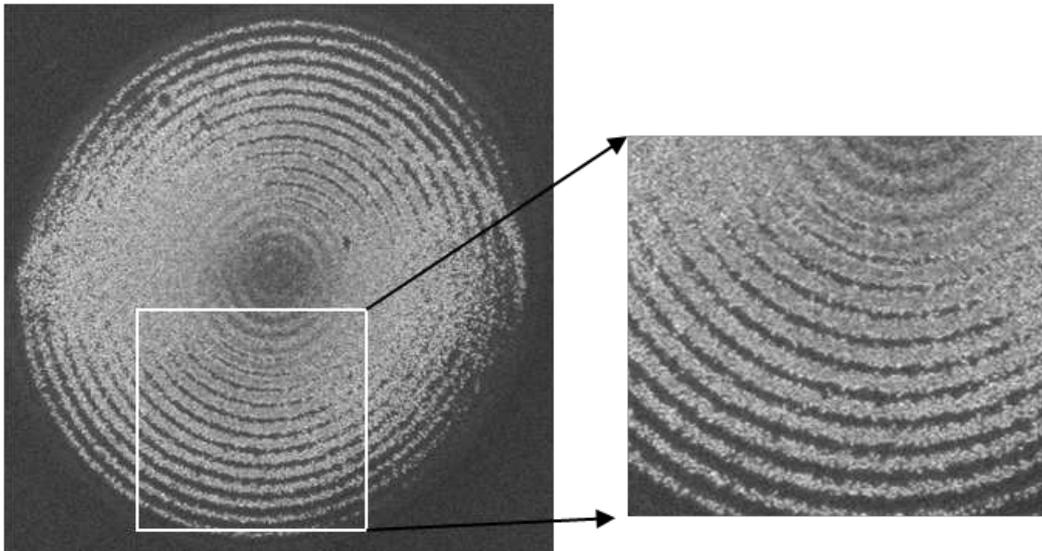
Figure 6. SEM images of copper deposited on two-photon patterned **SAM1**. The patterns are 40 μm in diameter and were fabricated using a tornado scanning mode with 10 μs·pixel^{-1}, 180 s of irradiation time and 62.2 mW of laser power.
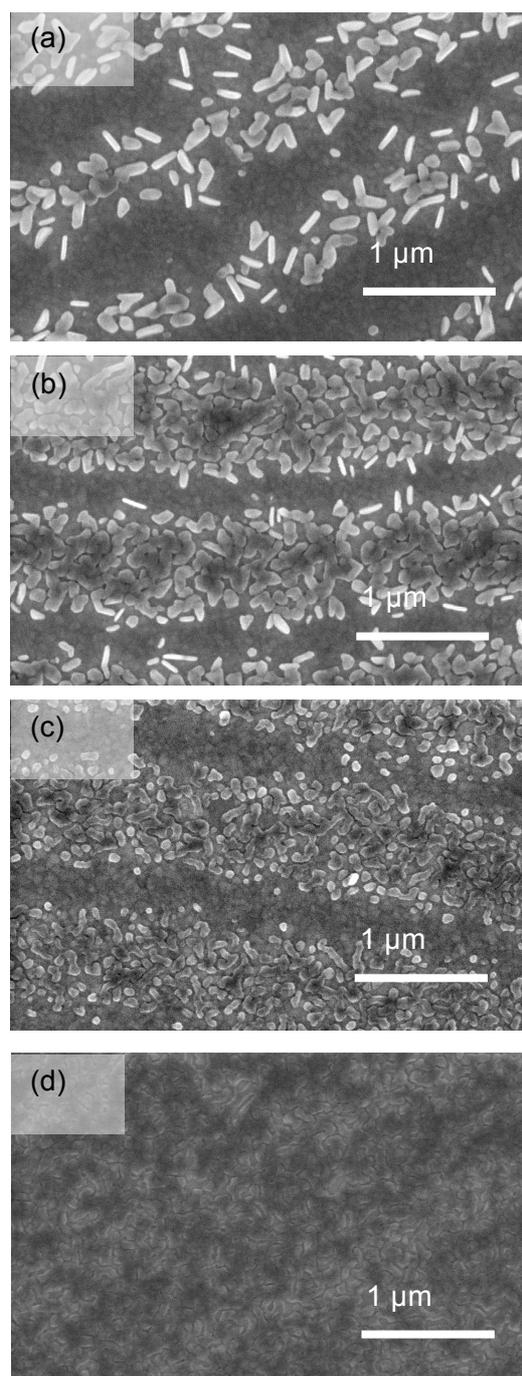
Figure 7. SEM images of copper deposited on two-photon patterned **SAM1**. (a) Laser power 62.2 mW, irradiation time 180 s. (b) Laser power 80.8 mW, irradiation time 180 s. (c) Laser power 62.2 mW, irradiation time 315 s. (d) Laser power 80.8 mW, irradiation time 315 s.

4. CONCLUSIONS

Photo-patterning of thiol-on-gold SAMs using soft UV (365 nm), can be used to make a surface suitable for selective and reversible electro-chemical deposition (ECD) of copper. The patterning of the SAMs is very stable and the features are reproducible over many cycles of copper deposition and copper removal. Unlike the case of densely packed SAMs, where the copper layer probably forms between the gold and the SAM and where the copper is relatively resistant to air oxidation, that deposited on the photolyzed surface, like copper deposited on bare gold, quite rapidly forms a surface film of copper oxide. Hence this copper layer probably forms above the SAM and this fact may help to explain the good reversibility of the process. Two-photon-induced photo-cleavage shows promise in terms of the ability to fabricate high-resolution patterns with sub-wavelength feature sizes.

ASSOCIATED CONTENT

Supporting Information

A movie showing the reversible deposition and removal of copper on a patterned SAM over the first two cycles. This material is available free of charge via the Internet at http://pubs.acs.org.

AUTHOR INFORMATION

Corresponding Author

*E-mail: S.D.Evans@leeds.ac.uk. Tel.: +44 113 343 3852.

Notes

The authors declare no competing financial interest.

REFERENCES

(1) Love, J. C.; Estroff, L. A.; Kriebel, J. K.; Nuzzo, R. G.; Whitesides, G. M. *Chem. Rev.* **2005**, *105*, 1103-1169.

(2) McCreery, R. L. *Chem. Mater.* **2004**, *16*, 4477-449

(3) Hipps, K. W. *Science* **2001**, *294*, 536-537.

(4) Cai, L. T.; Skulason, H.; Kushmerick, J. G.; Pollack, S. K.; Naciri, J.; Shashidhar, R.; Allara, D. L.; Mallouk, T. E.; Mayer, T. S. *J. Phys. Chem. B* **2004**, *108*, 2827-2832.

(5) Ozbay, E. *Science* **2006**, *311*, 189-193.

(6) J. Wang, J.; Zhu, T.; Song, J. Q.; Liu, Z. F. *Thin Solid Films* **1998**, *327*, 591-594.

(7) Ke, X.; Lu, B.; Hao, J.; Zhang, J.; Qiao, H.; Zhang, Z.; Xing, C.; Yang, W.; Zhang, B.; Tang, J. *ChemPhysChem* **2012**, *13*, 3786-3789.

(8) Volkel, B.; Kaltenpoth, G.; Handrea, M.; Sahre, M.; Nottbohm, C. T.; Kuller, A.; Paul, A.; Kautek, W.; Eck, W.; Golzhauser, A. *Surf. Sci.* **2005**, *597*, 32-41.

(9) Azzaroni, O.; Schilardi, P. L.; Salvarezza, R. C. *Appl. Phys. Lett.* **2002**, *80*, 1061-1063.

(10) Schilardi, P. L.; Azzaroni, O.; Salvarezza, R. C. *Langmuir* **2001**, *17*, 2748-2752.

(11) Schilardi, P. L.; Dip, P.; Claro, P. C. D.; Benitez, G. A.; Fonticelli, M. H.; Azzaroni, O.; Salvarezza, R. C. *Chem. Eur. J.* **2006**, *12*, 38-49.

(12) Sondag-Huethorst, J. A. M.; Fokkink, L. G. J. *Langmuir* **1995**, *11*, 4823-4831.

(13) Nishizawa, M.; Sunagawa, T.; Yoneyama, H. *Langmuir* **1997**, *13*, 5215-5217.

(14) Hagenstrom, H.; Schneeweiss, M. A.; Kolb, D. M. *Langmuir* **1999**, *15*, 7802-7809.

(15) Qu, D.; Uosaki, K. *J. Phys. Chem. B* **2006**, *110*, 17570-17577.

(16) Gilbert, S. E.; Cavalleri, O.; Kern, K. *J. Phys. Chem.* **1996**, *100*, 12123-12130.

(17) Hagenstrom, H.; Schneeweiss, M. A.; Kolb, D. M. *Electrochim. Acta* **1999**, *45*, 1141-1145.

(18) Cavalleri, O.; Gilbert, S. E.; Kern, K. *Chem. Phys. Lett.* **1997**, *269*, 479-484.

(19) Kaltenpoth, G.; Volkel, B.; Nottbohm, C. T.; Golzhauser, A.; Buck, M. *J. Vac. Sci. Technol., B* **2002**, *20,* 2734-2738.

(20) Silien, C.; Buck, M. *J. Phys. Chem. C* **2008**, *112*, 3881-3890.

(21) Baunach, T.; Ivanova, V.; Kolb, D. M.; Boyen, H. G.; Ziemann, P.; Buttner, M.; Oelhafen, P. *Adv. Mater.* **2004**, *16*, 2024-2028.

(22) Boyen, H. G.; Ziemann, P.; Wiedwald, U.; Ivanova, V.; Kolb, D. M.; Sakong, S.; Gross, A.; Romanyuk, A.; Buttner, M.; Oelhafen, P. *Nat. Mater.* **2006**, *5*, 394-399.

(23) Ivanova, V.; Baunach, T.; Kolb, D. A. *Electrochim. Acta* **2005**, *50*, 4283-4288.

(24) Felgenhauer, T.; Yan, C.; Geyer, W.; Rong, H. T.; Golzhauser, A.; Buck, M. *Appl. Phys. Lett.* **2001**, *79*, 3323-3325.

(25) Whelan, C. M.; Smyth, M. R.; Barnes, C. J. *J. Electroanal. Chem.* **1998**, *441*, 109-129.

(26) Batz, V.; Schneeweiss, M. A.; Kramer, D.; Hagenstrom, H.; Kolb, D. M.; Mandler, D. *J. Electroanal. Chem.* **2000**, *491*, 55-68.

(27) Moffat, T. P.; Yang, H. *Electrochem. Soc.* **1995**, *142*, L220-L222.

(28) Kumar, A.; Biebuyck, H. A.; Whitesides, G. M. *Langmuir* **1994**, *10*, 1498-1511.

(29) Pesika, N. S.; Radisic, A.; Stebe, K. J.; Searson, P. C. *Nano Lett.* **2006**, *6*, 1023-1026.

(30) Shi, Z.; Walker, A. V. *Langmuir* **2011**, *27*, 6932-6939.

(31) She, Z.; DiFalco, A.; Hähner, G.; Buck M. *Beilstein J. Nanotechnol.* **2012,** *3,* 101–113.

(32) Critchley, K.; Zhang, L. X.; Fukushima, H.; Ishida, M.; Shimoda, T.; Bushby, R. J.; Evans, S. D. *J. Phys. Chem. B* **2006**, *110*, 17167-17174.

(33) Jonas, U.; del Campo, A.; Kruger, C.; Glasser, G.; Boos, D. *Proc. Nat. Acad. Sci. U.S.A.* **2002**, *99*, 5034-5039.

(34) Critchley, K.; Jeyadevan, J. P.; Fukushima, H.; Ishida, M.; Shimoda, T.; Bushby, R. J.; Evans, S. D. *Langmuir* **2005**, *21*, 4554-4561.

(35) Prompinit, P.; Achalkumar, A. S.; Bramble, J. P.; Bushby, R. J.; Walti, C.; Evans, S. D. *ACS Appl. Mater. Interfaces* **2010**, *2*, 3686-3692.

(36) Prompinit, P.; Achalkumar, A. S.; Han, X. J.; Bushby, R. J.; Walti, C.; Evans, S. D. *J. Phys. Chem. C* **2009**, *113*, 21642-21647.

(37) Denk, W. *Proc. Nat. Acad. Sci. U.S.A.* **1994**, *91*, 6629-6633.

(38) Denk, W.; Strickler, J. H.; Webb, W. W. *Science* **1990**, *248*, 73-76.

(39) Pirrung, M. C.; Dore, T. M.; Zhu, Y.; Rana, V. S. *Chem. Commun.* **2010**, *46*, 5313-5315.

(40) Pirrung, M. C.; Pieper, W. H.; Kaliappan, K. P.; Dhananjeyan, M. R. *Proc. Nat. Acad. Sci. U.S.A.* **2003**, *100*, 12548-12553.

(41) Oheim, M.; Michael, D. J.; Geisbauer, M.; Madsen, D.; Chow, R. H. *Adv. Drug Delivery Rev.* **2006**, *58*, 788-808.

(42) Alvarez, M.; Best, A.; Pradhan-Kadam, S.; Koynov, K.; Jonas, U.; Kreiter, M. *Adv. Mater.* **2008**, *20*, 4563-4567.

(43) Alvarez, M.; Best, A.; Unger, A.; Alonso, J. M.; del Campo, A.; Schmelzeisen, M.; Koynov, K.; Kreiter, M. *Adv. Funct. Mater.* **2010**, *20*, 4265-4272.

(44) Monk, P. *Fundamentals of Electroanalytical Chemistry*; John Wiley: Chichester, 2001.

(45) Plambeck, J. A. *Electroanalytical Chemistry: Basic Principles and Applications*; Chichester : Wiley: New York, 1982.

(46) Azzaroni, O.; Schilardi, P. L.; Salvarezza R. C. *Electrochim. Acta* **2003**, *48*, 3107-3114.

(47) Paik, W. K.; Eu, S.; Lee, K.; Chon, S.; Kim, M. *Langmuir* **2000**, *16*, 10198-10205.

(48) Eu, S.; Paik, W. K. *Mol. Cryst. Liq. Cryst. Sci. Technol., Sect. A* **1999**, *337*, 49-52.

(49) Laibinis, P. E.; Whitesides, G. M. *J. Am. Chem. Soc.* **1992**, *114*, 9022-9028.

(50) Sung, M. M.; Sung, K.; Kim, C. G.; Lee, S. S.; Kim, Y. *J. Phys. Chem. B* **2000**, *104*, 2273-2277.

(51) Chavez, K. L.; Hess, D. W. *J. Electrochem. Soc.* **2001**, *148*, G640-G643.

(52) Dake, L. S.; King, D. E.; Czanderna, A. W. *Solid State Sci.* **2000**, *2*, 781-789.

(53) Zamborini, F. P.; Campbell, J. K.; Crooks, R. M. Spectroscopic, *Langmuir* **1998**, *14*, 640-647.

(54) Amato, C.; Devillers, S.; Calas, P.; Delhalle, J.; Mekhalif, Z. *Langmuir* **2008**, *24*, 10879-10886.

(55) Morales, J.; Sanchez, L.; Martin, F.; Ramos-Barrado, J.; Sanchez, M. *Thin Solid Films* **2005**, *474*, 133-140.

(56) Briggs, D.; Seah, M. P. *Practical Surface Analysis*; 2nd ed.; John Wiley & Son: New York, 1990; Vol. 1.

(57) Lin, S. Y.; Tsai, T. K.; Lin, C. M.; Chen, C. H.; Chan, Y. C.; Chen, H. W. *Langmuir* **2002**, *18*, 5473-5478.

(58) Sung, M. M.; Kim, Y. *Bull. Korean Chem. Soc.* **2001**, *22*, 748-752.

(59) Xing, J.-F; Dong, X.-Z.; Chen, W.-Q.; Duan, X.-M.; Takeyasu, N.; Tanaka, T.; Kawata S. *Appl. Phys. Lett.* **2007**, *90*, 131106.